Journal of Sound and Vibration (1999) **222**(5), 781–801
Article No. jsvi.1998.2134, available online at http://www.idealibrary.com on IDEAL®

ON THE SEPARATION BETWEEN MOVING VEHICLES AND BRIDGE

Y. S. Cheng, F. T. K. Au, Y. K. Cheung and D. Y. Zheng
Department of Civil Engineering, The University of Hong Kong, Pokfulam Road, Hong Kong

(*Received* 12 *June* 1998, *and in final form* 30 *November*, 1998)

In vehicle–bridge interaction problems, the contact force between the moving vehicle and the bridge depends on the velocity and acceleration of the moving vehicle, the flexibility of the bridge as well as the roughness of the upper surface of the bridge. In some cases, the contact force may become zero, which implies that the moving vehicle separates from the bridge. Neglecting this separation phenomenon will lead to a tensile contact force, which will affect the results. This paper investigates the onset and effects of separation between the moving vehicle and bridge. An algorithm to account for the impact on the re-establishment of contact is proposed. Numerical results also show that the effects are not negligible.

1. INTRODUCTION

The dynamic response of bridge structures subjected to moving vehicle loads has long been an interesting topic in the field of civil engineering. In particular, the interaction problem between vehicles and bridge structures has attracted much attention during the last two decades due to the large increase in the proportion of heavy vehicles and high-speed vehicles in highway and railway traffic. Fryba [1] has presented various analytical solutions for vibration problems of simply supported beams under moving vehicles. A number of semi-analytical methods have also been proposed for multi-span beam bridges using moving force models [2–5] or moving vehicle models [6]. However, in most of these studies, it has been implicitly assumed that the moving vehicle travelling on the bridge is always in contact with it, no matter what is the sign of the contact force. This is obviously not always true in view of the physics of the moving vehicle which simply sits on and slides along the upper surface of the bridge.

Figure 1 shows a vehicle modelled as a system of two degrees of freedom (DOFs), in which M_1 and M_2 are the unsprung mass and sprung mass of the moving vehicle, respectively. The vertical displacements of the unsprung mass M_1 and sprung mass M_2 with reference to their respective vertical equilibrium positions are $y_1(t)$ and $y_2(t)$, respectively. The horizontal position of the moving vehicle measured from a fixed point, such as the left end of the bridge, is $x(t)$.

0022–460X/99/200781 + 21 $30.00/0

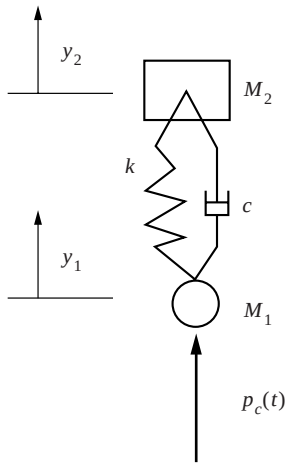

Figure 1. A vehicle modelled as a two-degree-of-freedom system.

The horizontal velocity and acceleration of the moving vehicle are v and a respectively. The vertical interaction force $p_c(t)$ acting on the moving vehicle can therefore be written as [6]:

$$p_c(t) = (M_1 + M_2)g + M_1 \frac{\mathrm{d}^2 y_1(t)}{\mathrm{d}t^2} + M_2 \frac{\mathrm{d}^2 y_2(t)}{\mathrm{d}t^2}, \tag{1}$$

in which g is the acceleration due to gravity. If there is no loss of contact between the unsprung mass and the upper surface of the bridge, the vertical displacement, velocity and acceleration of the unsprung mass can be taken respectively as

$$y_1(t) = [w(x, t) + r(x)]|_{x=x(t)} \tag{2}$$

$$\dot{y}_1(t) = \frac{\mathrm{d}y_1(t)}{\mathrm{d}t} = \left[\frac{\partial w}{\partial t} + v\frac{\partial w}{\partial x} + v\frac{dr}{dx}\right]\Bigg|_{x=x(t)} \tag{3}$$

$$\ddot{y}_1(t) = \frac{\mathrm{d}^2 y_1(t)}{\mathrm{d}t^2} = \left[\frac{\partial^2 w}{\partial t^2} + 2v\frac{\partial^2 w}{\partial x \partial t} + v^2\frac{\partial^2 w}{\partial x^2} + a\frac{\partial w}{\partial x} + v^2\frac{\mathrm{d}^2 r}{\mathrm{d}x^2} + a\frac{\mathrm{d}r}{\mathrm{d}x}\right]\Bigg|_{x=x(t)}, \tag{4}$$

where $w(x, t)$ is the upward deflection of the bridge and $r(x)$ is the surface roughness of the bridge which is defined as the vertically upward departure from the mean horizontal profile.

From equations (1) to (4), it can be seen that the interaction force between the moving vehicle and the bridge depends on the velocity and acceleration of the vehicle, the flexibility of the bridge and the roughness of the upper surface of the bridge. The interaction force does vary with time and it can be taken as an indicator of separation. When it becomes zero, it denotes the onset of separation, and it should remain zero until the moving vehicle re-establishes contact with the bridge.

Lee [7] has discussed the onset of separation between a moving mass and a beam. This paper further investigates the onset of separation and re-establishment of contact between the moving vehicle and the bridge. To minimize the error due to discretization, the dynamic stiffness method [8–10] is first utilized to obtain the "exact" frequencies and mode shapes of the bridge. Then the modal superposition method is coupled with the direct integration method to analyze the dynamic response of the bridge.

2. THEORY AND FORMULATION

A continuous linear elastic Bernoulli–Euler beam bridge with (n_s+1) point supports subjected to N moving vehicles is shown in Figure 2. The vehicles are modelled as moving systems each of 2 DOFs $\{M_{s1}, M_{s2}, c_s, k_s, s=1, 2, \ldots, N\}$, and they move as a group at a prescribed velocity $v(t)$ along the axial direction from left to right. Here M_{s1} and M_{s2} are the unsprung mass and sprung mass of the sth vehicle, respectively. The two masses are interconnected by a spring of stiffness k_s and a dashpot of damping coefficient c_s. The horizontal position of the sth vehicle measured from the left end of the bridge is $x_s(t)$, a function of time t. The deflection of the bridge is denoted by $w(x, t)$ where upward deflection is taken as positive. The vertical displacements of the masses M_{s1} and M_{s2} are $y_{s1}(t)$ and $y_{s2}(t)$, respectively, and they are measured vertically upward with reference to their respective vertical static equilibrium positions before they came onto the bridge.

2.1. DETERMINATION OF THE FREQUENCIES AND MODE SHAPES [8–10]

The governing equation for undamped flexural vibration $w(x, t)$ of a uniform beam is

$$EI\frac{\partial^4 w(x, t)}{\partial x^4} + \rho A\frac{\partial^2 w(x, t)}{\partial t^2} = 0 \tag{5}$$

where EI is the flexural stiffness, A is the cross-sectional area and ρ is the mass density. In particular, harmonic flexural vibration can be written as

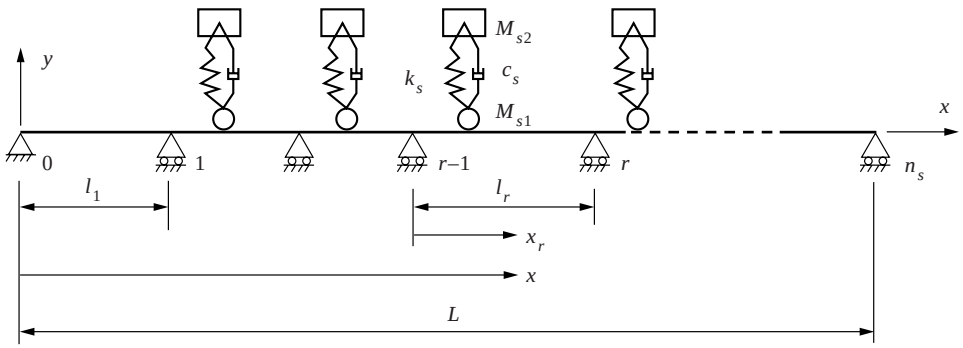

Figure 2. A continuous beam with (n_s+1) point supports under N moving vehicles.

$$w(x, t) = W(x)e^{i\omega t} \tag{6}$$

in terms of the mode shape $W(x)$ and the angular frequency ω. Using the method of separation of variables, one obtains

$$EI\frac{d^4W(x)}{dx^4} = \rho A\omega^2 W(x). \tag{7}$$

A multi-span continuous beam can be considered as an assemblage of a number of spans. The solution associated with the nodal displacements at the ends of a span

$$W|_{x=0} = u_1, \qquad \left.\frac{dW}{dx}\right|_{x=0} = u_2, \qquad W|_{x=l} = u_3 \quad \text{and} \quad \left.\frac{dW}{dx}\right|_{x=l} = u_4 \tag{8}$$

is therefore

$$W(x) = [N(x, \omega)][u_1 u_2 u_3 u_4]^T = \mathbf{N}(x, \omega)\mathbf{u}_e, \tag{9}$$

where the shape functions are

$$\mathbf{N}(x, \omega) = \begin{Bmatrix} \cos\lambda\xi \\ \sin\lambda\xi \\ \cosh\lambda\xi \\ \sinh\lambda\xi \end{Bmatrix}^T \begin{bmatrix} 1/2 - F_4/2\lambda^2 & F_2 l/2\lambda^2 & -F_3/2\lambda^2 & F_1 l/2\lambda^2 \\ -F_6/2\lambda^3 & l/2\lambda + F_4 l/2\lambda^3 & -F_5/2\lambda^3 & -F_3 l/2\lambda^3 \\ 1/2 + F_4/2\lambda^2 & -F_2 l/2\lambda^2 & F_3/2\lambda^2 & -F_1 l/2\lambda^2 \\ F_6/2\lambda^3 & l/2\lambda - F_4 l/2\lambda^3 & F_5/2\lambda^3 & F_3 l/2\lambda^3 \end{bmatrix}, \tag{10}$$

in which $\lambda^4 = \omega^2\rho A l^4/EI$, $\xi = x/l$, x is the local co-ordinate measured from the left end of the span and l is the length of the span. The frequency functions F_i are defined as

$$F_1 = -\lambda(\sinh\lambda - \sin\lambda)/\delta, \tag{11}$$

$$F_2 = -\lambda(\cosh\lambda\sin\lambda - \sinh\lambda\cos\lambda)/\delta, \tag{12}$$

$$F_3 = -\lambda^2(\cosh\lambda - \cos\lambda)/\delta, \tag{13}$$

$$F_4 = \lambda^2(\sinh\lambda\sin\lambda)/\delta, \tag{14}$$

$$F_5 = \lambda^3(\sinh\lambda + \sin\lambda)/\delta, \tag{15}$$

$$F_6 = -\lambda^3(\cosh\lambda\sin\lambda + \sinh\lambda\cos\lambda)/\delta, \tag{16}$$

$$\delta = \cosh\lambda\cos\lambda - 1. \tag{17}$$

Elements of the nodal force vector $\mathbf{Q}_e$ at the ends of the span are

$$Q_1 = EI\frac{\mathrm{d}^3 W}{\mathrm{d}x^3}\bigg|_{x=0},\quad Q_2 = -EI\frac{\mathrm{d}^2 W}{\mathrm{d}x^2}\bigg|_{x=0},\quad Q_3 = -EI\frac{\mathrm{d}^3 W}{\mathrm{d}x^3}\bigg|_{x=l}\quad \text{and}$$
$$Q_4 = EI\frac{\mathrm{d}^2 W}{\mathrm{d}x^2}\bigg|_{x=l}. \tag{18}$$

The nodal force vector $\mathbf{Q}_e$ and the nodal displacement vector $\mathbf{u}_e$ at the ends of the span are related by the beam element dynamic stiffness $\mathbf{d}(\omega^2)$ as

$$\mathbf{Q}_e = \mathbf{d}(\omega^2)\mathbf{u}_e. \tag{19}$$

By carrying out appropriate differentiation of the shape functions defined by equation (10), the beam element dynamic stiffness $\mathbf{d}(\omega^2)$ can be obtained as

$$\mathbf{d}(\omega^2) = \frac{EI}{l^3}\begin{bmatrix} F_6 & -F_4 l & F_5 & F_3 l \\ -F_4 l & F_2 l^2 & -F_3 l & F_1 l^2 \\ F_5 & -F_3 l & F_6 & F_4 l \\ F_3 l & F_1 l^2 & F_4 l & F_2 l^2 \end{bmatrix}. \tag{20}$$

The global dynamic stiffness matrix for the multi-span beam bridge shown in Figure 2 can therefore be assembled. After elimination of certain rows and columns to account for the boundary conditions, the governing equation for free vibration can be written as an eigenvalue problem

$$\mathbf{D}(\omega^2)\mathbf{U} = \mathbf{0}, \tag{21}$$

where $\mathbf{D}(\omega^2)$ is the global dynamic stiffness matrix and $\mathbf{U}$ is the global displacement vector defining the mode shapes. Non-trivial solutions to equation (21) can be determined by the following equation

$$\det(\mathbf{D}(\omega^2)) = 0. \tag{22}$$

Corresponding to each frequency ω_i, the mode shape $\phi_{ir}(x_r)$ of the rth span is given by

$$\phi_{ir}(x_r) = \mathbf{N}(x_r, \omega_i)\mathbf{u}_{er}, \tag{23}$$

where x_r is the local co-ordinate of the rth span and $\mathbf{u}_{er}$ is the displacement vector of the rth span for the ith mode shape.

If the global co-ordinate x is measured from the left end of the multi-span bridge, i.e.,

$$x = x_r + \sum_{j=1}^{r-1} l_j, \tag{24}$$

where l_j is the length of jth span, the ith mode shape in terms of the global co-

ordinate x can be written as

$$\Phi_i(x) = \phi_{ir}(x_r) \quad \text{for} \quad \sum_{j=1}^{r-1} l_j \leqslant x \leqslant \sum_{j=1}^{r} l_j, \qquad r = 1, 2, \ldots, n_s. \tag{25}$$

2.2. EQUATIONS OF MOTION IN MODAL CO-ORDINATES

After obtaining the natural frequencies and mode shapes by the dynamic stiffness method, the transverse deflection $w(x, t)$ of the bridge as shown in Figure 2 can be expressed as

$$w(x, t) = \sum_{i=1}^{n} q_i(t)\Phi_i(x), \tag{26}$$

where $(q_i(t),\ i = 1, 2, \ldots, n)$ are generalized co-ordinates to be determined, and $(\Phi_i(x),\ i = 1, 2, \ldots, n)$ are vibration mode shapes of the bridge considered.

Using the Lagrangian equation of the bridge and the constraint conditions at the contact points between the moving vehicles and the bridge (i.e., equations (2–4)), the equations of motion for the bridge can be written as follows [6].

$$\sum_{j=1}^{n} m_{ij}^{*}\ddot{q}_j(t) + \sum_{j=1}^{n} c_{ij}^{*}\dot{q}_j(t) + \sum_{j=1}^{n} k_{ij}^{*}q_j(t) + \sum_{s=1}^{N} M_{s2}\Phi_i(x_s(t))\ddot{y}_{s2}(t) = p_i^{*}(t),$$

$$i = 1, 2, \ldots, n, \tag{27}$$

where

$$m_{ij}^{*}(t) = m_{ij} + \sum_{s=1}^{N} M_{s1}\Phi_i(x_s(t))\Phi_j(x_s(t)), \tag{28}$$

$$m_{ij} = \int_0^L \rho A(x)\Phi_i(x)\Phi_j(x)\,\mathrm{d}x, \tag{29}$$

$$c_{ij}^{*}(t) = \sum_{s=1}^{N} 2vM_{s1}\Phi_i(x_s(t))\Phi_j'(x_s(t)), \tag{30}$$

$$k_{ij}^{*}(t) = k_{ij} + \sum_{s=1}^{N} M_{s1}\Phi_i(x_s(t))[v^2\Phi_j''(x_s(t)) + a\Phi_j'(x_s(t))], \tag{31}$$

$$k_{ij} = \int_0^L EI(x)\Phi_i''(x)\Phi_j''(x)\,\mathrm{d}x, \tag{32}$$

$$p_i^*(t) = -\sum_{s=1}^{N}[(M_{s1} + M_{s2})g\Phi_i(x_s(t)) + M_{s1}\Phi_i(x_s(t))(v^2 r''(x_s(t)) + ar'(x_s(t)))]. \tag{33}$$

In the above equations, the dot stands for differentiation with respect to time and the prime denotes differentiation with respect to x. Note that equation (27) is only valid under the condition that all N vehicles are acting on the bridge. Should a particular vehicle be outside the bridge, the corresponding terms under the summation signs should be omitted.

The equation of motion of the typical sprung mass M_{s2} is

$$M_{s2}\,\ddot{y}_{s2}(t) + c_s(\,\dot{y}_{s2}(t) - \dot{y}_{s1}(t)) + k_s(\,y_{s2}(t) - y_{s1}(t)) = 0. \tag{34}$$

Substituting equations (2–4) and (26) into equation (34), the equation of motion of the typical sprung mass M_{s2} becomes

$$-\sum_{j=1}^{n} c_s\Phi_j(x_s(t))\dot{q}_j(t) - \sum_{j=1}^{n}[k_s\Phi_j(x_s(t)) + vc_s\Phi_j'(x_s(t))]q_j(t)$$
$$+ M_{s2}\,\ddot{y}_{s2}(t) + c_s\,\dot{y}_{s2}(t) + k_s\,y_{s2}(t) = k_s r(x_s(t)) + vc_s r'(x_s(t)),$$
$$s = 1, 2, \ldots, N. \tag{35}$$

Again the above equation is only valid when the sth vehicle acts on the bridge.

Equations (27) and (35) can be written together in matrix form as

$$\begin{bmatrix} \mathbf{M}^* & \Phi\mathbf{M}_2 \\ \mathbf{0} & \mathbf{M}_2 \end{bmatrix}\begin{Bmatrix} \ddot{\mathbf{q}} \\ \ddot{\mathbf{y}}_2 \end{Bmatrix} + \begin{bmatrix} \mathbf{C}^* & \mathbf{0} \\ -\mathbf{C}\Phi^{\mathrm{T}} & \mathbf{C} \end{bmatrix}\begin{Bmatrix} \dot{\mathbf{q}} \\ \dot{\mathbf{y}}_2 \end{Bmatrix} + \begin{bmatrix} \mathbf{K}^* & \mathbf{0} \\ -\mathbf{K}\Phi^{\mathrm{T}} - v\mathbf{C}\Phi'^{\mathrm{T}} & \mathbf{K} \end{bmatrix}\begin{Bmatrix} \mathbf{q} \\ \mathbf{y}_2 \end{Bmatrix}$$
$$= \begin{Bmatrix} \mathbf{p}^* \\ \mathbf{K}\mathbf{r} + v\mathbf{C}\mathbf{r}' \end{Bmatrix}, \tag{36}$$

where the sub-matrices are given below in terms of the typical element at the ith row and the jth column, and the sub-vectors are given in terms of the typical ith element

$$\mathbf{M}^* = [m_{ij}^*(t)], \quad \mathbf{C}^* = [c_{ij}^*(t)], \quad \mathbf{K}^* = [k_{ij}^*(t)], \qquad i, j = 1, 2, \ldots, n, \tag{37–39}$$

$$\mathbf{M}_2 = \mathrm{diag}[M_{i2}], \quad \mathbf{C} = \mathrm{diag}[c_i], \quad \mathbf{K} = \mathrm{diag}[k_i], \qquad i = 1, 2, \ldots, N, \tag{40–42}$$

$$\Phi = [\Phi_i(x_j(t))], \qquad i = 1, 2, \ldots, n;\ j = 1, 2, \ldots, N, \tag{43}$$

$$\mathbf{p}^* = \{p_i^*(t)\}, \quad \mathbf{q} = \{q_i(t)\}, \qquad i = 1, 2, \ldots, n, \tag{44, 45}$$

$$\mathbf{r} = \{r(x_i(t))\}, \quad \mathbf{y}_2 = \{y_{i2}(t)\}, \qquad i = 1, 2, \ldots, N. \tag{46, 47}$$

Equation (36) can then be solved by the Wilson-θ method [11] or a similar technique. Likewise, this equation has been written on the assumption that all N

vehicles are acting on the bridge. Where a certain vehicle is not on the bridge, the corresponding rows and columns of the matrix equation should be deleted.

2.3. SEPARATION AND RE-ESTABLISHMENT OF CONTACT BETWEEN VEHICLE AND BRIDGE

As mentioned above, the vertical interaction force acting on the moving vehicle $p_c(t)$ can be monitored to find out when separation occurs. If the sth vehicle separates from the bridge during the time interval $t_1 \leqslant t \leqslant t_2$, then the vehicle undergoes unconstrained motion under gravity and the equations of motion of the entire vehicle–bridge system need to be modified. In particular, the motion of the unsprung mass of that vehicle no longer follows the upper surface of the bridge and hence the displacement of the unsprung mass $y_1(t)$ should be separately solved.

Consider the special case in which only one vehicle acts on the bridge. During the brief time interval ($t_1 \leqslant t \leqslant t_2$) of separation, the bridge is under free vibration with initial conditions at $t = t_1$. In other words, the equation of motion of the bridge can be written as

$$\mathbf{M}_b\ddot{\mathbf{q}} + \mathbf{K}_b\mathbf{q} = \mathbf{0}, \tag{48}$$

with the initial conditions specified as

$$\mathbf{q} = \{q_i(t_1)\}, \quad \dot{\mathbf{q}} = \{\dot{q}_i(t_1)\}, \qquad i = 1, 2, \ldots, n \tag{49}$$

where the mass matrix $\mathbf{M}_b$ and the stiffness matrix $\mathbf{K}_b$ of the bridge are respectively

$$\mathbf{M}_b = [m_{ij}], \quad \mathbf{K}_b = [k_{ij}], \qquad i, j = 1, 2, \ldots, n. \tag{50}$$

The equation of motion of the vehicle which separates from the bridge can be written as

$$\begin{bmatrix} M_1 & 0 \\ 0 & M_2 \end{bmatrix} \begin{Bmatrix} \ddot{y}_1(t) \\ \ddot{y}_2(t) \end{Bmatrix} + \begin{bmatrix} c & -c \\ -c & c \end{bmatrix} \begin{Bmatrix} \dot{y}_1(t) \\ \dot{y}_2(t) \end{Bmatrix} + \begin{bmatrix} k & -k \\ -k & k \end{bmatrix} \begin{Bmatrix} y_1(t) \\ y_2(t) \end{Bmatrix} = \begin{Bmatrix} -M_1 g \\ -M_2 g \end{Bmatrix}, \tag{51}$$

with the initial displacements and velocities of the unsprung and sprung masses specified at the time $t = t_1$ when the vehicle first separates from the bridge. In particular, the initial displacement and velocity of the unsprung mass are

$$y_1(t_1) = [w(x, t) + r(x)]\Big|_{\substack{x=x_1(t_1) \\ t=t_1}}, \tag{52}$$

$$\dot{y}_1(t_1) = \left[\frac{\partial w(x, t)}{\partial t} + v\frac{\partial w(x, t)}{\partial x} + v\frac{\mathrm{d}r(x)}{\mathrm{d}x}\right]\Bigg|_{\substack{x=x_1(t_1) \\ t=t_1}}, \tag{53}$$

where $x_1(t)$ is the position of the vehicle. Note that equation (2) will not be true during the time interval of separation. Contact between the vehicle and the bridge is re-established at $t = t_2$ when the displacement of the unsprung mass $y_1(t_2)$ obtained from equation (51) becomes equal to the bridge deflection

$w(x_1(t_2), t_2) + r(x_1(t_2))$ again. Numerically, this condition can be detected from the following inequalities where applicable

$$\left.\frac{|y_1(t) - (w(x, t) + r(x))|}{\min(|y_1(t)|, |w(x, t) + r(x)|)}\right|_{\substack{x=x_1(t_2)\\ t=t_2}} \leqslant \varsigma_1, \tag{54}$$

$$1 - \varsigma_2 \leqslant \left.\frac{y_1(t)}{w(x, t) + r(x)}\right|_{\substack{x=x_1(t_2)\\ t=t_2}} \leqslant 1 \quad \text{for} \quad \begin{matrix} y_1(t_2) > 0 \\ w(x_1(t_2), t_2) + r(x_1(t_2)) > 0 \end{matrix}, \tag{55}$$

$$1 - \varsigma_3 \leqslant \left.\frac{|w(x, t) + r(x)|}{|y_1(t)|}\right|_{\substack{x=x_1(t_2)\\ t=t_2}} \leqslant 1 \quad \text{for} \quad \begin{matrix} y_1(t_2) < 0 \\ w(x_1(t_2), t_2) + r(x_1(t_2)) < 0 \end{matrix}, \tag{56}$$

$$\max\left((w(x, t) + r(x))\Big|_{\substack{x=x_1(t_2)\\ t=t_2}}, |y_1(t)|_{t=t_2} \right) \leqslant \varsigma_4 \quad \text{for} \quad \begin{matrix} y_1(t_2) < 0 \\ w(x_1(t_2), t_2) + r(x_1(t_2)) > 0 \end{matrix}, \tag{57}$$

in which ς_i are small positive parameters which depend on the accuracy required. Then using the displacements and velocities at $t = t_2$ as initial conditions, the equation of motion for the vehicle–bridge system shown in equation (36) can be used again to solve for the subsequent dynamic response.

2.4. IMPACT ON RE-ESTABLISHMENT OF CONTACT BETWEEN VEHICLE AND BRIDGE

In the solution of equation (36) for the subsequent dynamic response after re-establishment of contact between the vehicle and bridge, the initial displacements and velocities are required. However, the velocities of the unsprung mass and the bridge at the point of contact are normally different, and an impact is inevitable. If impact is neglected, one may assume that the velocity distribution along the bridge is hardly affected, and the distribution of displacements and velocities of the bridge at $t = t_2$ can be taken as initial conditions.

In this paper, it is assumed that the impact force $P_{im}(t)$ of very short duration can be approximated by

$$P_{im}(t) = p_{im} p(t), \tag{58}$$

where $p(t)$ is an assumed distribution of time history with maximum magnitude of unity and p_{im} is the maximum impact force to be determined. As the duration of the impact Δt is very short, the change of horizontal position of the vehicle during impact can be neglected. Under these simplifying assumptions, the impact problem is equivalent to finding the maximum impact force p_{im} and the duration of impact Δt such that the displacements and velocities of the vehicle and bridge at the end of the impact duration are compatible and that the interaction force is continuous. It has also been implicitly assumed that violation of compatibility of displacements and velocities within the very short impact duration is ignored.

For simplicity of argument, only one vehicle is assumed to act on the bridge. Under the above assumptions, the equation of motion for the vehicle during the impact time interval $t_2 \leqslant t \leqslant t_2 + \Delta t$ can be written as

$$\begin{bmatrix} M_1 & 0 \\ 0 & M_2 \end{bmatrix} \begin{Bmatrix} \ddot{y}_1 \\ \ddot{y}_2 \end{Bmatrix} + \begin{bmatrix} c & -c \\ -c & c \end{bmatrix} \begin{Bmatrix} \dot{y}_1 \\ \dot{y}_2 \end{Bmatrix} + \begin{bmatrix} k & -k \\ -k & k \end{bmatrix} \begin{Bmatrix} y_1 \\ y_2 \end{Bmatrix} = \begin{Bmatrix} P_{im}(t) \\ 0 \end{Bmatrix}, \quad (59)$$

with the initial displacements and velocities taken as those at time $t = t_2$, i.e., $y_1(t_2)$, $y_2(t_2)$, $\dot{y}_1(t_2)$ and $\dot{y}_2(t_2)$. Similarly the equation of motion for the bridge in the same impact time interval becomes

$$\mathbf{M}_b\ddot{\mathbf{q}} + \mathbf{K}_b\mathbf{q} = \mathbf{P}, \quad (60)$$

with the initial conditions specified as

$$\mathbf{q} = \{q_i(t_2)\}, \ \dot{\mathbf{q}} = \{\dot{q}_i(t_2)\}, \qquad i = 1, 2, \ldots, n, \quad (61)$$

where the force vector due to the impact is

$$\mathbf{P} = \{-P_{im}(t)\Phi_i(x_1(t_2))\}, \qquad i = 1, 2, \ldots, n. \quad (62)$$

At the end of the brief impact time interval, the displacements and velocities of the vehicle and bridge at the contact point should be compatible, and hence

$$y_1(t_2 + \Delta t) = [w(x, t) + r(x)]\Big|_{\substack{x=x_1(t_2) \\ t=t_2+\Delta t}}, \quad (63)$$

$$\dot{y}_1(t_2 + \Delta t) = \left[\frac{\partial w(x, t)}{\partial t} + v\frac{\partial w(x, t)}{\partial x} + v\frac{\mathrm{d}r(x)}{\mathrm{d}x}\right]\Bigg|_{\substack{x=x_1(t_2) \\ t=t_2+\Delta t}}. \quad (64)$$

The continuity of the interaction force can be ensured by using an impact force distribution function $P_{im}(t)$ which is continuous with the subsequent interaction force, and it can be approximately enforced by iterations. For example, the assumed continuous impact force time history may be taken as

$$P_{im}(t) = \begin{cases} 0 & t = t_2 \\ p_1(t) & t_2 < t < t_2 + \beta\Delta t \\ p_{im} & t = t_2 + \beta\Delta t \\ p_2(t) & t_2 + \beta\Delta t < t < t_2 + \Delta t \\ p_{c0} & t = t_2 + \Delta t \end{cases}, \quad (65)$$

where $p_1(t)$ and $p_2(t)$ are assumed functions, β is an assumed positive parameter which is less than one, p_{im} is the maximum impact force and p_{c0} is an assumed interaction force at the end of the impact time interval, as shown in Figure 3.

The search for suitable control variables p_{im}, p_{c0} and Δt is itself an optimization problem with constraints. The problem is to minimize the objective function $F(p_{im}, \Delta t)$

$$F(p_{im}, \Delta t) = \left| \dot{y}_1(t) - \left(\frac{\partial w(x, t)}{\partial t} + v\frac{\partial w(x, t)}{\partial x} + v\frac{\mathrm{d}r(x)}{\mathrm{d}x}\right)\Bigg|_{\substack{x=x_1(t_2) \\ t=t_2+\Delta t}} \right| \quad (66)$$

subject to the following constraints governing displacements where applicable:

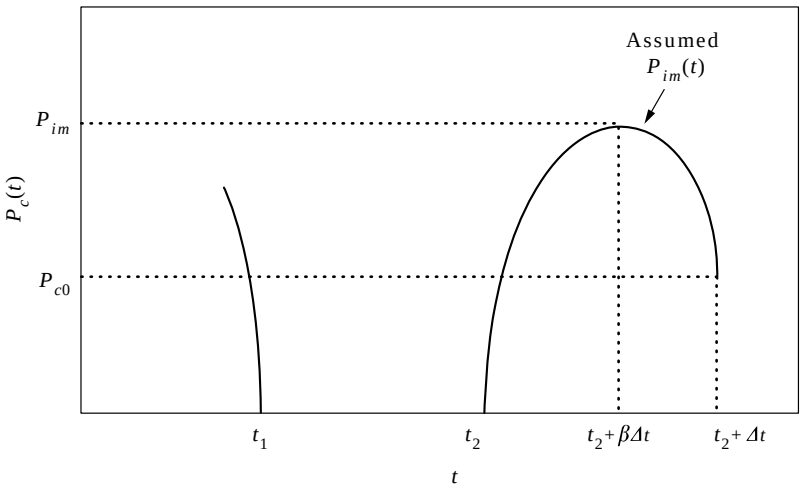

Figure 3. Assumed time history of interaction force on separation and re-establishment of contact between vehicle and bridge.

$$\left.\frac{|y_1(t)-(w(x,\,t)+r(x))|}{\min(|y_1(t)|,\,|w(x,\,t)+r(x)|)}\right|_{\substack{x=x_1(t_2)\\ t=t_2+\Delta t}} \leqslant \varepsilon_1, \tag{67}$$

$$1-\varepsilon_2 \leqslant \left.\frac{y_1(t)}{w(x,\,t)+r(x)}\right|_{\substack{x=x_1(t_2)\\ t=t_2+\Delta t}} \leqslant 1 \quad \text{for} \quad \begin{matrix} y_1(t_2+\Delta t)>0 \\ w(x_1(t_2),\,t_2+\Delta t)+r(x_1(t_2))>0 \end{matrix}, \tag{68}$$

$$1-\varepsilon_3 \leqslant \left.\frac{|w(x,\,t)+r(x)|}{|y_1(t)|}\right|_{\substack{x=x_1(t_2)\\ t=t_2+\Delta t}} \leqslant 1 \quad \text{for} \quad \begin{matrix} y_1(t_2+\Delta t)<0 \\ w(x_1(t_2),\,t_2+\Delta t)+r(x_1(t_2))<0 \end{matrix}, \tag{69}$$

$$\max\left((w(x,\,t)+r(x))\Big|_{\substack{x=x_1(t_2)\\ t=t_2+\Delta t}},\,|y_1(t)|_{t=t_2+\Delta t}\right) \leqslant \varepsilon_4 \quad \text{for} \quad \begin{matrix} y_1(t_2+\Delta t)<0 \\ w(x_1(t_2),\,t_2+\Delta t)+r(x_1(t_2))>0 \end{matrix}, \tag{70}$$

and the following constraints governing velocities and interaction force

$$\left.\left(\dot{y}_1(t)\cdot\left(\frac{\partial w(x,\,t)}{\partial t}+v\frac{\partial w(x,\,t)}{\partial x}+v\frac{\mathrm{d}r(x)}{\mathrm{d}x}\right)\right)\right|_{\substack{x=x_1(t_2)\\ t=t_2+\Delta t}} > 0, \tag{71}$$

$$\left.\frac{\left|\dot{y}_1(t)-\left(\dfrac{\partial w(x,\,t)}{\partial t}+v\dfrac{\partial w(x,\,t)}{\partial x}+v\dfrac{\mathrm{d}r(x)}{\mathrm{d}x}\right)\right|}{\max\left(|\dot{y}_1(t)|,\,\left|\dfrac{\partial w(x,\,t)}{\partial t}+v\dfrac{\partial w(x,\,t)}{\partial x}+v\dfrac{\mathrm{d}r(x)}{\mathrm{d}x}\right|\right)}\right|_{\substack{x=x_1(t_2)\\ t=t_2+\Delta t}} \leqslant \varepsilon_5, \tag{72}$$

$$\left|\frac{p_{c0} - p_c}{p_{c0}}\right| < \varepsilon_6, \tag{73}$$

in which ε_i are small positive parameters controlling the required computing accuracy and the actual interaction force p_c can be obtained from equation (1). Note that the above constraints are introduced to account for various possible conditions. After formulating the problem, any appropriate algorithm for non-linear constrained optimization can be applied for its solution.

Notice that in the search for re-establishment of contact alone, only geometric compatibility needs to be considered. However, to take into account the impact as well, it is necessary to consider both the geometric compatibility and velocity compatibility between the unsprung mass and the bridge.

3. NUMERICAL RESULTS

Figure 4 shows a single-span simply supported bridge which may have a harmonically varying surface irregularity represented by

$$r(x) = (d/2)(1 - \cos(2\pi x/\bar{l})), \tag{74}$$

where d and $\bar{\ell}$ are the surface irregularity depth and length, respectively. A vehicle, which is modelled as an unsprung mass m_1 and a sprung mass m_2 interconnected by a spring with stiffness k and a damper with damping coefficient c, is assumed to move with a constant speed v along the bridge. In parallel with the notations used in reference [12], seven dimensionless parameters are defined as follows: velocity ratio, $\alpha = v\pi/\omega_{b,1}l$, where $\omega_{b,1} = \pi^2\sqrt{EI/\rho Al^4}$; unsprung to sprung mass ratio, $\kappa_0 = m_1/m_2$; vehicle to bridge mass ratio, $\kappa = (m_1 + m_2)/\rho Al$; bridge to vehicle frequency ratio, $\Omega = \omega_{b,1}/\omega_v$, where $\omega_v = \sqrt{k/m_2}$; vehicle damping ratio, $\zeta_v = c/2m_2\omega_v$; surface irregularity depth ratio, $r_d = -48EId/(m_1 + m_2)gl^3$; and surface irregularity length ratio, $r_l = l/\bar{l}$. The velocity ratio α is defined in such a way that, when α equals unity, the vehicle traversing time $\tau = l/v$ equals half the fundamental period of the bridge.

For comparison with reference [12], the following specific parameters are assumed: $\kappa = 0{\cdot}5$, $\kappa_0 = 0{\cdot}25$, $\Omega = 3$ and $\xi_v = 0{\cdot}125$. Various cases of the velocity

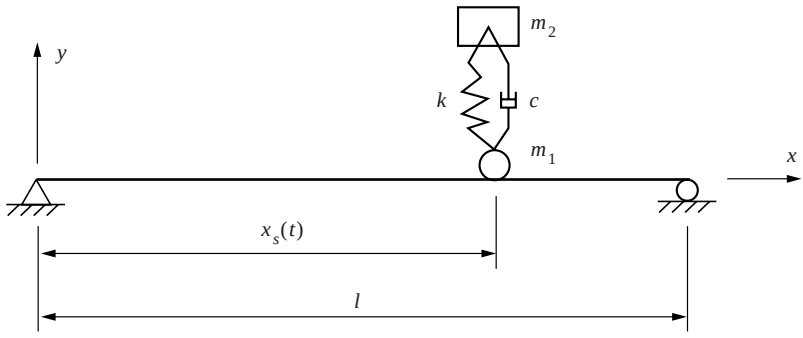

Figure 4. A single-span simply supported bridge under a single-axle moving vehicle.

ratios α and roughness are considered. The problem was solved by the present method using eight vibration modes and 200 equal time steps. The parameter θ used in the Wilson-θ method was taken to be 1·4. In the presentation of results, the dynamic magnification factors for mid-span displacement D_d and mid-span bending moment D_m are defined as: D_d = (maximum dynamic mid-span displacement)/(static mid-span displacement); and D_m = (maximum dynamic mid-span moment)/(static mid-span moment), where the static quantities equal $-(m_1+m_2)gl^3/48EI$ and $(m_1+m_2)gl/4$, respectively, due to a concentrated load $(m_1+m_2)g$ placed at mid-span.

A perfectly smooth bridge (i.e., $r_d=r_l=0$) was first analyzed, and Figures 5 and 6 show the dynamic magnification factors D_d and D_m respectively for the range of velocity ratio $0 \leqslant \alpha \leqslant 1{\cdot}0$. No separation between vehicle and bridge was detected. Then the same bridge with roughness ($r_d=0{\cdot}05$, $r_l=10$) was studied, and the dynamic magnification factors D_d and D_m for the range of velocity ratio $0 \leqslant \alpha \leqslant 0{\cdot}5$ are shown in Figures 7 and 8, respectively. Again no separation between vehicle and bridge was detected within this range of velocity ratio. In general, good agreement is observed between the present results and those due to Olsson [12]. However, some discrepancies in the results for the dynamic magnification factor D_m are noticed as the computed bending moment, being proportional to the second derivative of the deflection with respect to co-ordinate x, is very much dependent on the numerical method used. The dynamic stiffness method adopted in the present approach is expected to be more accurate provided that sufficient vibration modes have been used.

In the case of the bridge with roughness, separation between vehicle and bridge is expected for higher values of velocity ratio. In order to study the effects

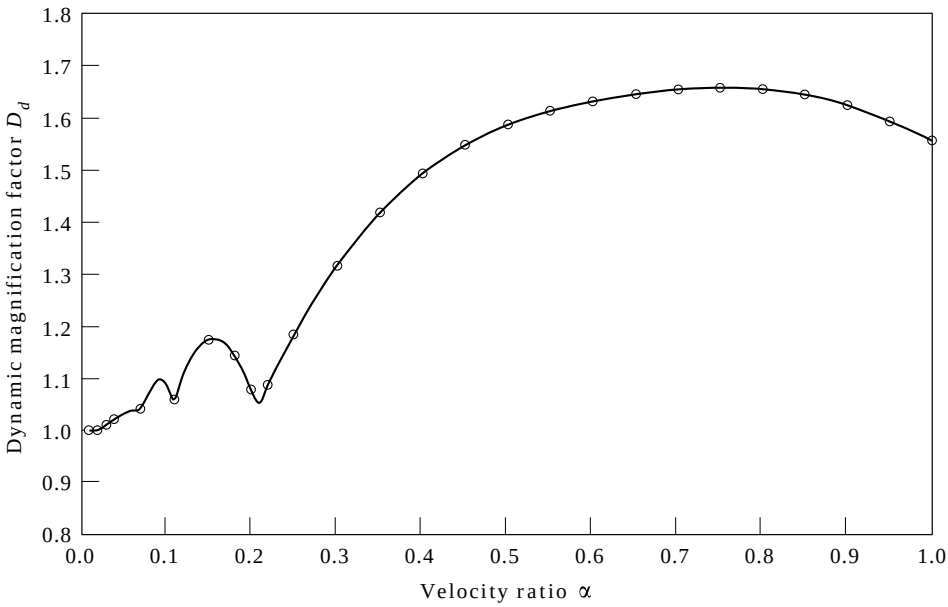

Figure 5. Simply supported bridge without roughness under a vehicle, dynamic magnification factor D_d. —, Present; ○, reference [12].

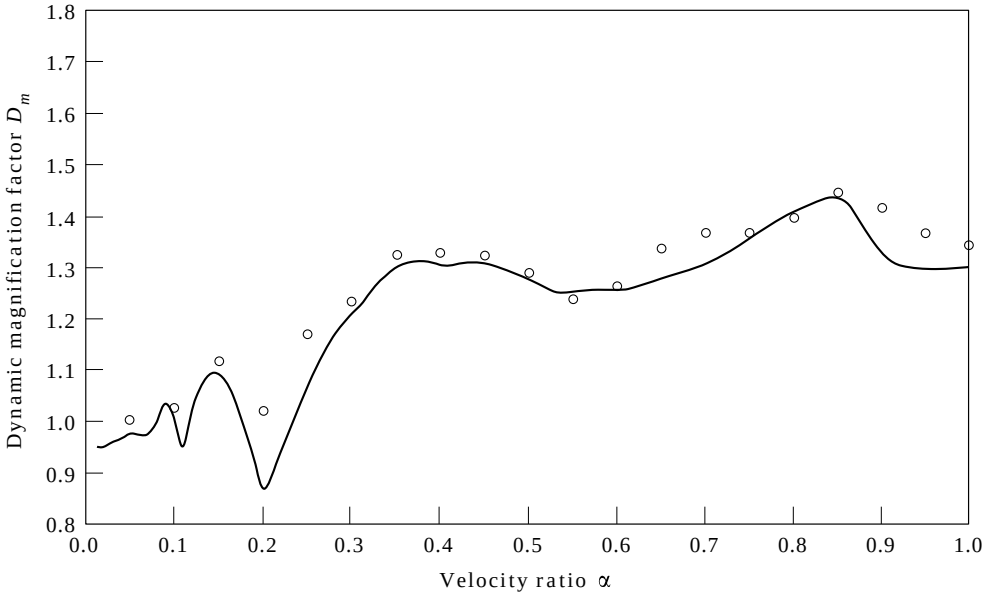

Figure 6. Simply supported bridge without roughness under a vehicle, dynamic magnification factor D_m. Key as for Figure 5.

of separation and impact on the bridge dynamics, the above bridge was re-analyzed for the following assumptions: (a) separation between vehicle and bridge is ignored; (b) separation between vehicle and bridge is considered but the impact on re-establishment of contact is ignored; and (c) both separation and impact on re-establishment of contact between vehicle and bridge are considered.

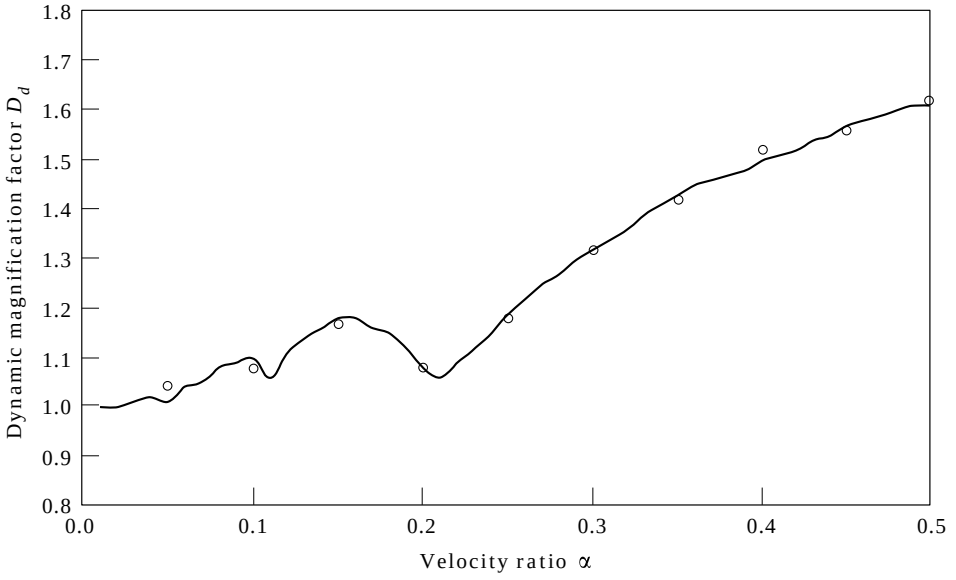

Figure 7. Simply supported bridge with roughness under a vehicle, dynamic magnification factor D_d. Key as for Figure 5.

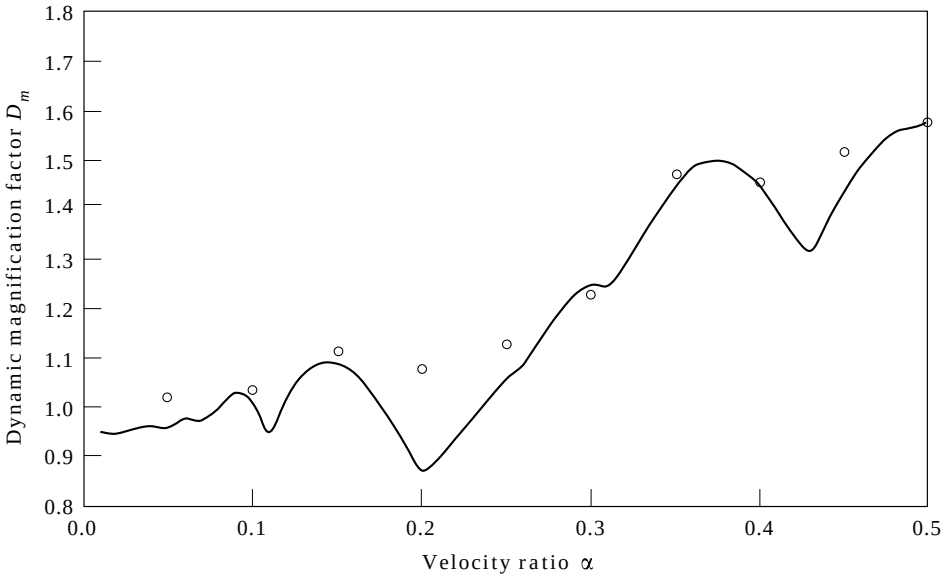

Figure 8. Simply supported bridge with roughness under a vehicle, dynamic magnification factor D_m. Key as for Figure 5.

When separation and subsequent re-establishment of contact between vehicle and bridge are considered, the following parameters are used: $\varsigma_1 = \varsigma_2 = \varsigma_3 = 0{\cdot}05$; $\varsigma_4 = 10^{-5}$ m; $\varepsilon_1 = \varepsilon_2 = \varepsilon_3 = \varepsilon_5 = \varepsilon_6 = 0{\cdot}05$; and $\varepsilon_4 = 10^{-5}$ m. The assumed impact force time history $P_{im}(t)$ is shown in Figure 9 and defined as follows:

$$p_{im}(t) = \begin{cases} \dfrac{p_{im} \cdot (t - t_2)}{0{\cdot}5\Delta t} & \text{for} \quad t_2 \leqslant t \leqslant t_2 + 0{\cdot}5\Delta t, \\ p_{im} - \dfrac{(p_{im} - p_{c0})}{0{\cdot}5\Delta t} \cdot (t - t_2 - 0{\cdot}5\Delta t) & \text{for} \quad t_2 + 0{\cdot}5\Delta t \leqslant t \leqslant t_2 + \Delta t. \end{cases} \tag{75}$$

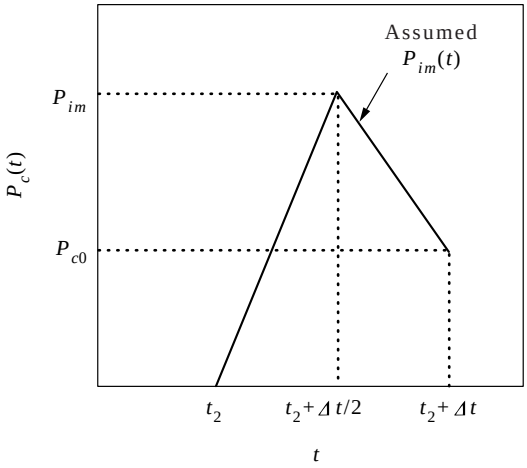

Figure 9. Assumed time history of impact force on re-establishment of contact between vehicle and bridge used in numerical example.

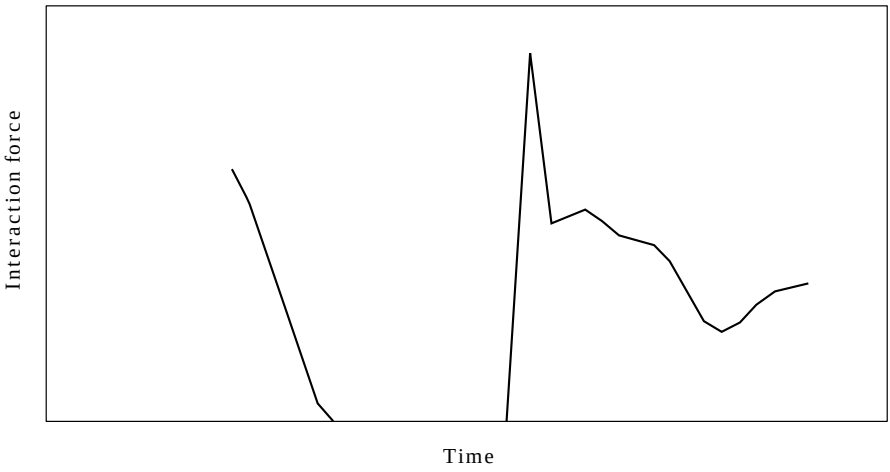

Figure 10. Simply supported bridge with roughness under a vehicle, typical interaction force prior to and after separation.

The method of constrained variable metric [13] was employed to solve the constrained optimization problem described in the last section. A typical time history of interaction force prior to and after separation is shown in Figure 10. It shows the fairly concentrated impact force following re-establishment of contact between the vehicle and bridge. The full time histories of interaction forces obtained from various assumptions are shown in Figure 11. Note that the impact forces on re-establishment of contact have not been plotted here as these time histories are plotted along regular time intervals. It shows that if the separation between the vehicle and bridge is ignored, tensile interaction forces

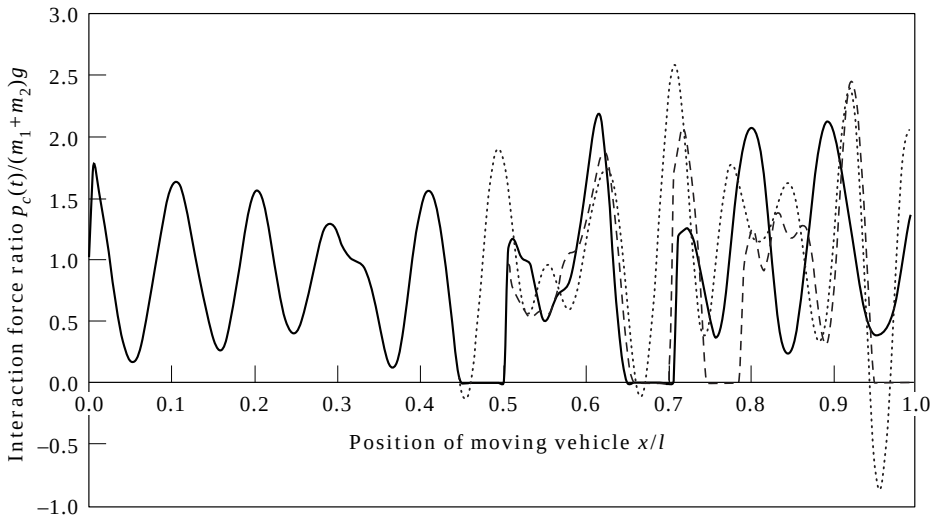

Figure 11. Simply supported bridge with roughness under a vehicle, interaction force ratio calculated from different schemes. – – –, (a) Separation ignored; — — —, (b) separation considered but impact ignored; ——, (c) both separation and impact considered.

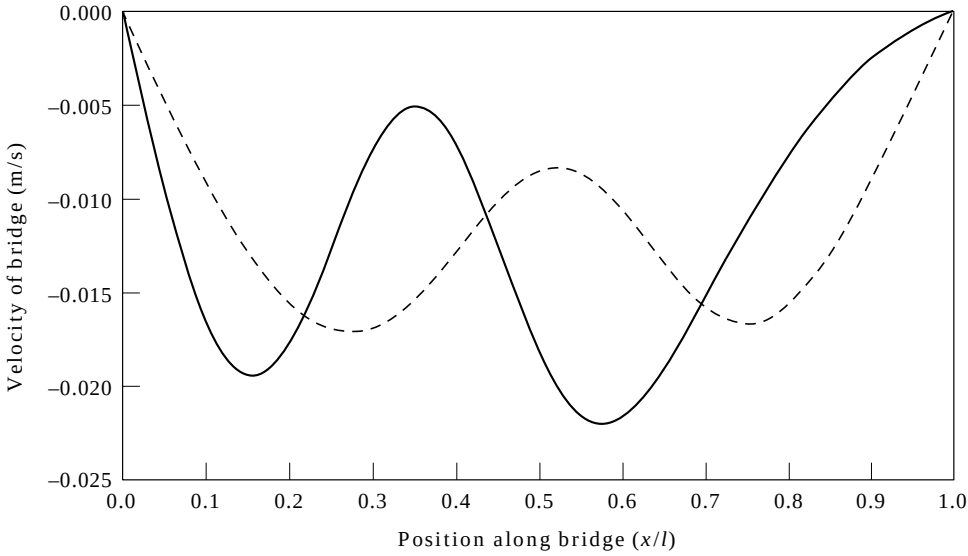

Figure 12. Velocity distribution of bridge immediately before and after re-establishment of contact between the vehicle and bridge roughly at mid-span position for velocity ratio $\alpha = 0{\cdot}64$. ——, Velocity after impact; – – – –, velocity before impact.

may result, which is physically impossible. One major effect of the impact on re-establishment of contact between the vehicle and bridge is the change in velocity distribution along the length of the bridge. Figure 12 shows the velocity distributions immediately before and after the impact that occurs roughly at mid-span position for the velocity ratio $\alpha = 0{\cdot}64$. It is observed that the velocity

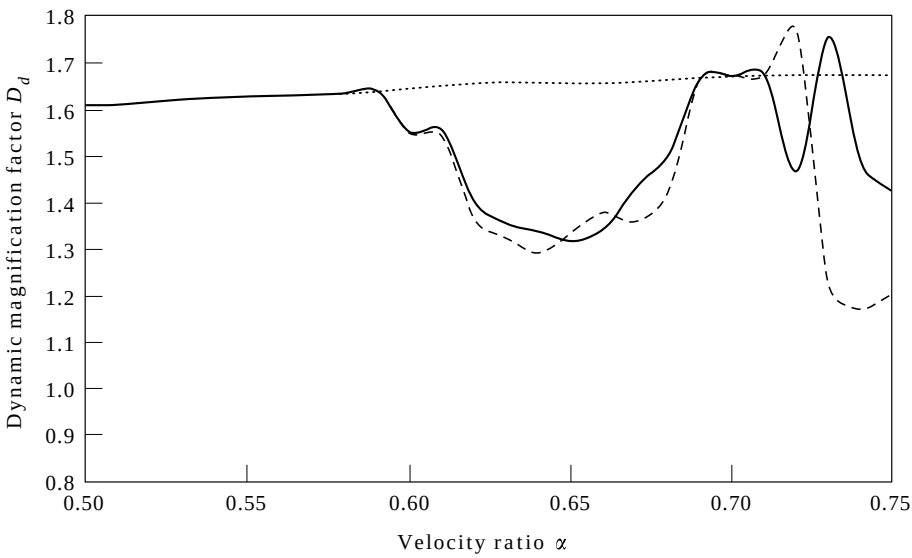

Figure 13. Simply supported bridge with roughness under a vehicle, dynamic magnification factor D_d. Key as for Figure 11.

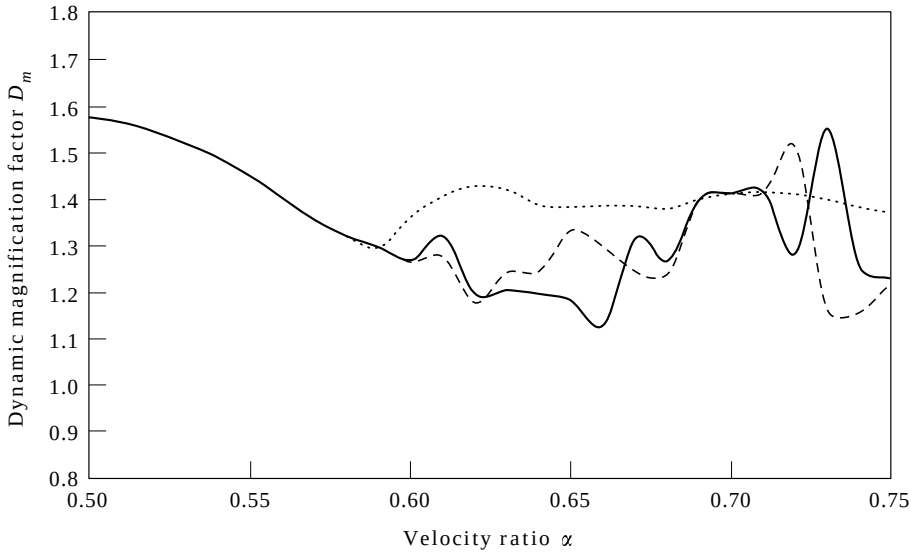

Figure 14. Simply supported bridge with roughness under a vehicle, dynamic magnification factor D_m. Key as for Figure 11.

distribution has been radically altered. As the velocity distribution serves as one of the initial conditions for subsequent solution of the problem, it shows that the effects of impact should be considered in order to obtain an accurate picture of the bridge response.

The dynamic magnification factors D_d and D_m are computed for the range of velocity ratio ($0{\cdot}5 \leqslant \alpha \leqslant 0{\cdot}75$) under various assumptions, and shown in Figures 13 and 14, respectively. The effect of impact on these dynamic magnification factors is apparent. Separation between vehicle and bridge is observed for

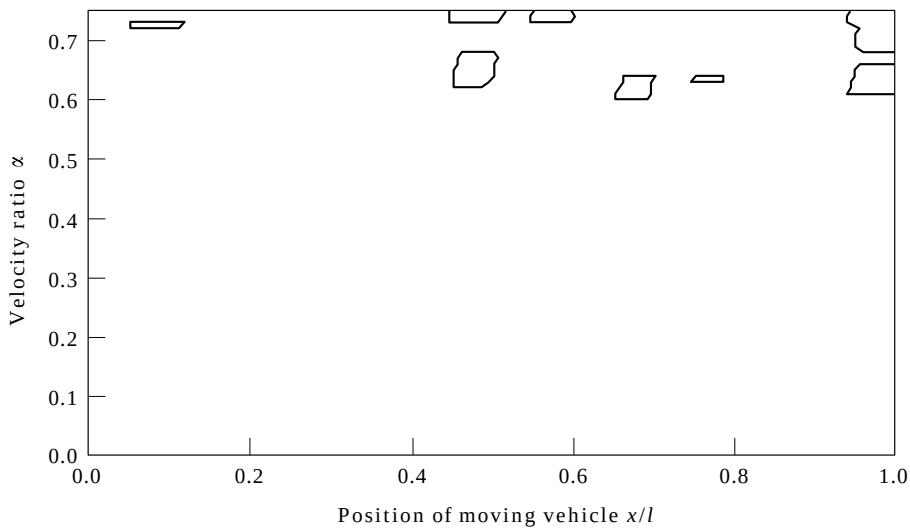

Figure 15. Simply supported bridge with roughness under a vehicle, separation region obtained with impact ignored.

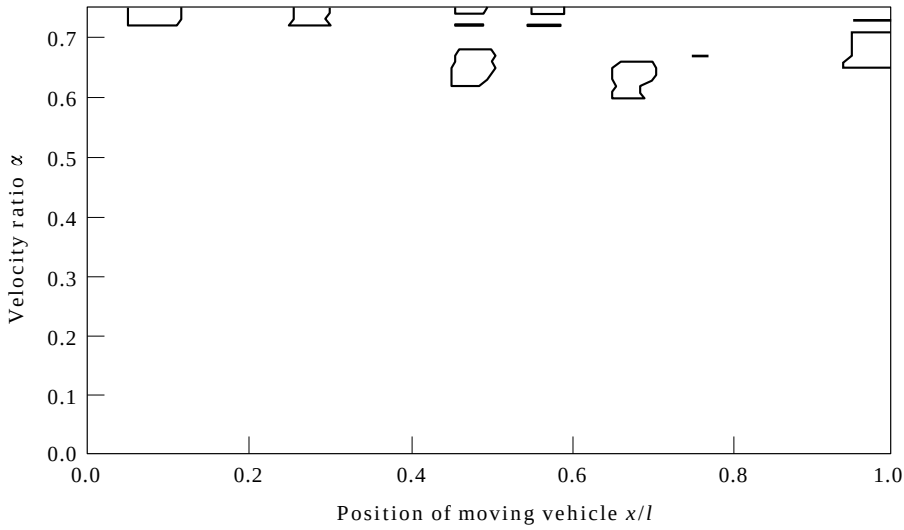

Figure 16. Simply supported bridge with roughness under vehicle, separation region obtained with impact considered.

velocity ratios approximately above 0·59. Beyond this point, the curves in each figure tend to diverge. However, in the range of velocity ratio ($0{\cdot}69 \leqslant \alpha \leqslant 0{\cdot}71$), the curves tend to converge again. This is because the vehicle separates from the bridge only after creating the maximum deflection or bending moment.

The regions along the bridge in which the separation between the moving vehicle and bridge occurs are shown in Figure 15 for the case when only separation is considered and in Figure 16 for the case when both separation and impact are considered. It is observed that separation between the moving vehicle and bridge often occurs in the vicinity of the crests of roughness. Figures 15 and 16 show that no separation occurs below certain values of the velocity ratio. However, as the velocity of the vehicle increases, separation occurs more often and the separation region seems to widen and appear earlier.

4. CONCLUSION

This paper investigates the vehicle–bridge interaction problem taking into account the effects of separation and impact on re-establishment of contact between the moving vehicle and bridge. The use of the dynamic stiffness method for evaluation of the natural frequencies and mode shapes of the bridge has provided a sound basis for subsequent analysis using modal superposition. Time history analysis of the vehicle–bridge system is then carried out with a direct integration algorithm which can take into account the separation and impact on re-establishment of contact between the moving vehicle and bridge. It is observed that separation often occurs in the vicinity of the crests of roughness. In the examples considered, it is observed that no separation occurs below certain values of the velocity ratio. As the velocity of the vehicle increases, separation occurs more often and the separation region seems to widen and appear earlier. The velocity distribution of the bridge is also radically altered by

the impact force. To ensure an accurate estimation of the dynamic response of a vehicle–bridge system, the effects of separation and impact should be taken into account.

5. ACKNOWLEDGMENT

The financial support of the Hong Kong Research Grants Council is acknowledged.

REFERENCES

1. L. FRYBA 1972 *Vibration of Solids and Structures Under Moving Loads*. Groningen, The Netherlands: Noordhoff International Publishing.
2. T. HAYASHIKAWA and N. WATANABE 1981 *Journal of Structural Mechanics Division, American Society of Civil Engineers* **107**, 229–246. Dynamic behavior of continuous beams with moving loads.
3. J. S. WU and C. W. DAI 1987 *Journal of Structural Engineering* **113**, 458–474. Dynamic responses of multi-span nonuniform beam due to moving loads.
4. K. HENCHI, M. FAFARD, G. DHATT and M. TALBOT 1997 *Journal of Sound and Vibration* **199**, 33–50. Dynamic behavior of multi-span beams under moving loads.
5. D. Y. ZHENG, Y. K. CHEUNG, F. T. K. AU and Y. S. CHENG 1998 *Journal of Sound and Vibration* **212**, 455–467. Vibration of multi-span non-uniform beams under moving loads by using modified beam vibration functions.
6. Y. K. CHEUNG, F. T. K. AU, D. Y. ZHENG and Y. S. CHENG (under review) Vibration of multi-span non-uniform bridges under moving vehicles by using modified beam vibration functions.
7. U. LEE 1996 *Journal of Vibration and Acoustics* **118**, 517–521. Revisiting the moving mass problem: onset of separation between the mass and beam.
8. T. H. RICHARDS and Y. T. LEUNG 1977 *Journal of Sound and Vibration* **55**, 363–376. An accurate method in structural vibration analysis.
9. A. Y. T. LEUNG 1993 *Dynamic Stiffness and Substructures*. London: Springer.
10. N. J. FERGUSSON 1991 *Ph.D. thesis, University of Virginia*. The free and forced vibrations of structures using the finite dynamic element method.
11. K. J. BATHE and E. L. WILSON 1976 *Numerical Methods in Finite Element Analysis*. Englewood Cliffs, NJ: Prentice-Hall.
12. M. OLSSON 1985 *Journal of Sound and Vibration* **99** 1–12. Finite element, modal co-ordinate analysis of structures subjected to moving loads.
13. J. YU and J. ZHOU 1989 *Optimization Programmes OPB-1: Theory and Applications* (in Chinese). Beijing, PR China: Mechanical Industry Press.

APPENDIX: A: NOTATION

$\{c_s, s=1, 2, \ldots, N\}$	damping coefficient of the sth vehicle
$EI(x)$	flexural rigidity of the bridge
$\{k_s, s=1, 2, \ldots, N\}$	stiffness of the spring of the sth vehicle
$\{m_{ij}, k_{ij}, i, j=1, 2, \ldots, n\}$	generalized mass and stiffness matrices of the bridge only
$\{m^*_{ij}, c^*_{ij}, k^*_{ij}, i, j=1, 2, \ldots, n\}$	generalized mass, damping and stiffness matrices of the vehicle–bridge system

$\{M_{s1}, M_{s2}, s=1, 2, \ldots, N\}$	unsprung mass and sprung mass, respectively, of the sth vehicle
n_s	n_s is the number of spans
N	number of vehicles in the convoy
$p_c(t)$	interaction force between the vehicle and the bridge
$\{p_i^*(t), i=1, 2, \ldots, n\}$	generalized force
$P_{im}(t)$	time history of impact force
$\{q_i(t), i=1, 2, \ldots, n\}$	generalized co-ordinates of the bridge
$r(x)$	surface irregularity function
Δt	impact period
$v(t)$	velocity of the convoy
x_r	local abscissa of the rth span
$\{x_s(t), s=1, 2, \ldots, N\}$	abscissa of the sth vehicle
$w(x, t)$	deflection of the bridge at position x
$\{y_{s1}(t), y_{s2}(t), s=1, 2, \ldots, N\}$	vertical displacements of the unsprung mass and sprung mass, respectively, of the sth vehicle
ω	natural frequency of the bridge
$\phi_{ir}(x_r)$	the ith vibration mode of the rth span
$\{\Phi_i(x), i=1, 2, \ldots, n\}$	the ith vibration mode of the bridge
$\rho A(x)$	mass per unit length of the bridge
$\mathbf{D}(\omega^2)$	global dynamic stiffness matrix
$\mathbf{M}^*$, $\mathbf{C}^*$, $\mathbf{K}^*$	generalized mass, damping and stiffness matrices of the vehicle–bridge system
$\mathbf{M}_2$, $\mathbf{C}$, $\mathbf{K}$	vehicle unsprung mass, damping and stiffness matrices
$\mathbf{M}_b$, $\mathbf{K}_b$	mass and stiffness matrices of the bridge
$\mathbf{p}$	generalized force vector during impact
$\mathbf{p}^*$	generalized force vector
$\mathbf{q}$	generalized co-ordinate vector for the bridge
$\mathbf{r}$	surface irregularity function vector
$\mathbf{y}_2$	vehicle sprung mass displacement vector
Φ	vibration mode shape matrix